frontiers | Frontiers in Physics

TYPE Original Research
PUBLISHED 16 November 2022
DOI 10.3389/fphy.2022.1032437

OPEN ACCESS

EDITED BY
Kh. S. Mekheimer,
Al-Azhar University, Egypt

REVIEWED BY
Sankar M,
University of Technology and Applied Sciences, Oman
Rushi Kumar B,
VIT University, India

*CORRESPONDENCE
Arshad Riaz,
arshad-riaz@ue.edu.pk

SPECIALTY SECTION
This article was submitted to Statistical and Computational Physics, a section of the journal Frontiers in Physics

RECEIVED 30 August 2022
ACCEPTED 20 October 2022
PUBLISHED 16 November 2022

CITATION
Bilal S, Khan NZ, Riaz A, Alyami MA and El-Din EMT (2022), Measure and evaluate the hydrothermal flow of a Newtonian fluid in homogeneous permeable media equipped with a fin: A numerical approach.
Front. Phys. 10:1032437.
doi: 10.3389/fphy.2022.1032437

Measure and evaluate the hydrothermal flow of a Newtonian fluid in homogeneous permeable media equipped with a fin: A numerical approach

Sardar Bilal[1], Noor Zeb Khan[1], Arshad Riaz[2]*, Maryam Ahmed Alyami[3] and ElSayed M. Tag El-Din[4]

[1]Department of Mathematics, Air University, Islamabad, Pakistan, [2]Department of Mathematics, Division of Science and Technology, University of Education, Lahore, Pakistan, [3]Department of Mathematics, Faculty of Sciences, University of Jeddah, Jeddah, Saudi Arabia, [4]Center of Research, Faculty of Engineering, Future University in Egypt, New Cairo, Egypt

This study envisions the hydrothermal characteristics of a viscous fluid in a homogenously permeable hexagonal enclosure. Permeability aspects in the flow domain are described by employing the Brinkman-extended Darcy law. A corrugated hexagonal enclosure along with the placement of a star-shaped fin is taken into account. Heated rectangular blocks at horizontal extremities are installed, and sliding sides of the enclosure are considered to be cold to provide convective potential to the flow. In addition, adjoining portions of the heated rectangular blocks are supposed to be adiabatic. The dimensionless governing equations of the resultant problem are derived initially and then solved numerically by implementing the Galerkin finite element approach, and COMSOL is obliged. For this purpose, first, domain discretization is demonstrated in view of 2D elements by performing hybridized meshing. Then, the system of non-linear equations is resolved by a non-linear solver (PARADISO). The grid convergence test is performed to confirm the credibility of the carried out simulations by calculating the average Nusselt number at different refinement levels. A change in associated distributions against the involved physical parameters (Darcy number (Da), Rayleigh number (Ra), and Prandtl number (Pr)) for a wide range is revealed through graphs and tables. Quantities like kinetic energy and heat flux (local and average) are also evaluated through concerned parameters. The results clearly demonstrate that the Darcy number tends to reduce the heat transfer rate. In particular, it is depicted that by increasing the Rayleigh number (Ra), strengthening in the temperature potential arises in the system, thereby magnifying the heat transfer rate. Moreover, it is disclosed that by reducing the Darcy number, kinetic energy shows a decreasing trend.

KEYWORDS

permeable media, natural convection, hexagonal cavity, cold fin, FEM, Newtonian fluid

Introduction

A medium composing of gaps and voids is usually renowned as permeable. On the basis of connections between voids, permeable media are classified into saturated and unsaturated media. Transport of liquids through permeable media has been an area of interest in numerous fields such as hydrological systems, thermal insulation, filtering procedures, pollutant removal, resource engineering, drying procedures, storage of liquefied gases, solidification of castings, biofilm growth, and fuel cells. In 1856, Darcy wrote a book related to the concept of flow mechanics in permeable media by depicting the transport of water through beds of sand. This book laid down the basis for researchers working in this direction, and later on, Darcy proposed a law representing the relation for the velocity profile depending on the pressure at a low Reynold number. Brinkman [1] calculated the viscous force influenced by a flowing liquid in the permeable medium and developed the momentum equation according to Darcy's law. Beavers and Joseph [2] developed boundary conditions generated between the interaction of fluid in permeable and homogenous media. Poulikakos [3] contemplated the convective flow of a liquid on a permeable bed by employing the Darcy model. Beckermann et al. [4] anticipated free convective thermal transport between a permeable layer and fluid inside a rectangular enclosure. Beckermann et al. [5] manifested the convective flow of a viscous liquid in a rectangular cavity with solidification effects. Chen and Chen [6] probed experimental analysis on a superposed fluid in a permeable layer over a horizontal surface. Breton [7] studied convective thermal transport in a square enclosure with differentially heated vertical extremities immersed in a permeable medium by employing control volume formulation. Singh et al. [8] presented the computational modeling of 3D convective flow immersed in permeable layers by formulating the Brinkman-extended Darcy relation. Webster et al. [9] disclosed the exchange of solutes in a sedimental flow in a permeable medium. Goyeau et al. [10] conducted momentum transfer at the interface of permeable and homogeneous domains by employing the jump condition and developing a volume-averaged equation. Nessrine et al. [11] employed a non-Darcian relation to investigate the thermal attributes of the fluid in a permeable pipe. Kemparaju et al. [12] examined thermosolutal flow in a porous annulus with horizontal impermeable boundaries and insulated vertical extremities. Reddy et al. [13] investigated buoyantly driven flow of nanoliquid in a porous annular region by taking into account the adiabatic inner cylinder. They discovered that uplift in the permeability constant intensifies the movement of nanoparticles in a porous annulus.

Convective energy transport in saturated permeable media has enchanted a receivable focus due to extensive relevance in numerous utilizations like in heat sinks, heat exchangers, catalytic reactors, and mechanical energy absorbers. In addition, free convective flow through permeable media possesses noticeable industrial employments such as thermal insulation, washing machines, drying procedures, biomedical engineering, and nuclear reactors [14]. In addition, convective transport through permeable media is of specified interest in geological and geophysical processes [15, 16]. In view of such extraordinary applicability, a great deal of studies has been conducted. For example, Molla et al. [17] studied the natural convection generated by fluid flow in a saturated porous enclosure with localized heating and by providing symmetric heat distribution. Alhashah and Saleh [18] elucidated the influence of permeability on convective flow in an enclosure filled with water containing Cu particles by employing the Darcy law.

Optimization in a natural convection process in enclosures by installing heated or cold baffles is an effective strategy and utilized in multiple thermodynamical systems. Through experimentations, it is proved that the use of baffles has played a vital role in increasing the efficiency of heat-exchange systems by producing extraordinary convective diffusions. In addition, the appropriate adjustment of baffles is important in maintenance of fluid in thermodynamical equilibrium. Some recent studies conducted in this direction are Abedini et al. [19] who examined the thermal characteristics of a magnetically affected convective viscous liquid in a C-shaped enclosure with the installation of baffles. They measured the increase in heat flux by varying the aspect ratio of baffles. Jetli et al. [20] demonstrated the natural convective flow in a partially differentiated square enclosure by changing the location of the baffles. They examined that the heat flux decreases as the space between two baffles increases. Armaghani et al. [21] illustrated entropy generation in water by adding alumina particles in a T-shaped enclosure with baffles. They proposed that by increasing the aspect ratio of baffles, diffusion of nanoparticles along with elevation in heat and mass diffusions occur. Free convective flow in a inclined rectangular enclosure by varying the baffle length was represented by Hussein et al. [22]. They described that by enhancing the size of baffles, flow and thermal transport in the computational domain gradually increase. Buoyantly driven flow in nanoliquid with placement of V- and H-shaped baffles in the enclosure was scrutinized by Keramat et al. [23]. An increase in the heat transmission rate by installing heated baffles and by making improvisation in the magnitude of the Rayleigh number was measured by Nia et al. [24]. The influence of length and positioning of the baffle on convective flow in an L-shaped enclosure was discussed by Ghalambaz et al. [25]. It was concluded that a stiffer baffle reduces the convective thermal transport by resisting fluid flow. Performance of hybrid nanofluid with the placement of a heated baffle in a ventilated enclosure was examined by Du et al. [26]. Zadeh et al. [27] determined the impact of the gap ratio of placed baffles and change in height on the average heat flux coefficient for the flow viscous liquid in an enclosure. The mixed convective heat-transfer phenomenon in a square enclosure by changing the magnitude of the Reynold number and baffle gap was elucidated by Hussain et al. [28]. Benzenin et al. [29] demonstrated the influence of baffles on controlling the

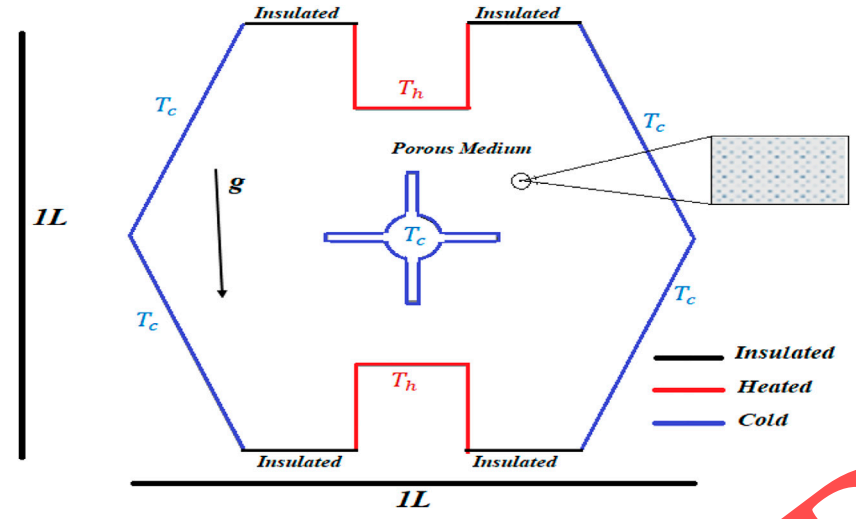

FIGURE 1
Diagrammatic representation of the problem.

turbulence generated in air flow by considering flat and rectangular baffles. Saravanan and Vidhya [30] examined heat transfer with the placement of heat-generating thin vertical baffles in a square enclosure and by placing baffles at different positions. Thermosolutal convection in a permeable annulus with a thin baffle attached to the inner cylinder was observed by Pushpa et al. [31]. They found that the reduction in the length of the baffle reduces mass and heat transport rates. Some additional studies demonstrating the characteristics of heat transfer and mass transfer in an annulus with thin baffles and different materials were manifested by [32–34].

The property of liquids which identifies the response of shear stress is known as viscosity. It is the intrinsic characteristic of every material that differentiates it from others. On the basis of viscosity and shear-stress relationship, fluids are characterized into Newtonian and non-Newtonian liquids. The basic and essential constituents of nature on which life is dependent are air and water. These components of nature are Newtonian in properties and execute linear deformation scaling against the stress. Applications of air and water are found in each walk of life, but some procedures involving them extensively are as coolants in automobiles, air filters, removal of nuclear wastage, drying of fibrous materials, pulp suspensions, and in the human blood circulatory system. Dazodzo and Dazodzo [35] elucidated the flow and thermal characteristics of water with a temperature gradient produced by convective forces in an enclosure. Backermann et al. [36] performed an investigation into the naturally convective flow of water in a permeable vertical cavity by measuring quantities of interest (kinetic energy, local, and average heat fluxes) versus Rayleigh number (Ra) and Prandtl number (Pr). The impact of permeability on viscous liquid flow in a rectangular enclosure along with the assumption of convective forces for low magnitude of flow-controlling parameters was determined by Ali et al. [37]. The onset about instability in creeping flow of air in a cavity with centrally localized heaters was illustrated by Torance and Rockett [38]. The latest available studies on Newtonian liquid flow in different domains are shown in refs [39–42].

From the thorough review of the available literature related to convective thermal transport in a closed domain, it is observed that simple configurations are taken into account. Since most of the physical phenomena occurring in nature are complexed in nature and demand for complex domains, this article is manipulated by taking into account the physical importance of such configurations. In addition, the placement of complicated fins to reduce or supply appropriate heat in the thermal exchange procedure is required, so in view of it, essence fin is also assumed in the current work. Physical aspects of permeability and convection are also considered to raise the practical utilization of this study. It is also concluded from the examination of accessible studies that very scant work has been carried out in this direction, and no study on this domain has been conducted so far. From the authors' consensus, this work is novel and will definitely provide direction to researchers.

The novelty of the present work is itemized as follows:

- Consideration of a complex domain (hexagonal cavity) with a corrugated rectangular block on boundaries and a cold star-shaped fin.
- Natural convection generated by density and gravity differences.
- The Darcy model is invoked in the problem to adumbrate permeability effects.
- A cold fin is installed to measure optimized change in convection.

TABLE 1 Mesh statistics against different refinement levels.

Refinement level	No. of elements	D.O.F
Level-1	626	3,997
Level-2	858	5,493
Level-3	1,052	6,687
Level-4	1,482	9,201
Level-5	2,750	16,453
Level-6	3,874	22,633
Level-7	6,184	35,135
Level-8	13,948	77,399
Level-9	33,604	1,82,259

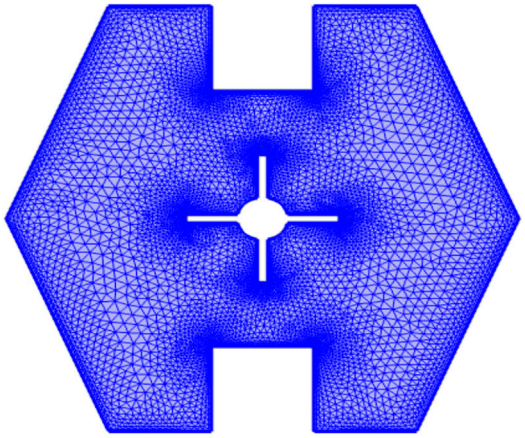

FIGURE 2
Extra-fine grid for the cavity with a fin placed.

Mathematical description

Problem description

Let us assume an incompressible, steady and 2D flow of a viscous fluid filled in a hexagonal enclosure. Density is considered to vary with change in gravity force and employed in modeling by taking into account the Boussinesq approximation. Permeability aspects are also obliged by incorporating the Brinkman-extended Darcy model. Two rectangles are corrugated at lower and upper horizontal walls of the enclosure by providing uniform heating, whereas the adjoining portion is assumed to be adiabatic. A star-shaped fin is placed at the center of the enclosure and prescribed with zero temperature to enhance thermal convective potential (Figure 1).

Governing models

By considering aforementioned assumptions, the governing equations are represented as follows ref [43].

$$u_{\tilde{X}} + v_{\tilde{Y}} = 0, \tag{1}$$

$$uu_{\tilde{X}} + vu_{\tilde{Y}} = -\frac{1}{\rho}p_{\tilde{X}} + v\left[u_{\tilde{X}\tilde{X}} + u_{\tilde{Y}\tilde{Y}}\right] - \frac{v}{\kappa}u, \tag{2}$$

$$uv_{\tilde{X}} + vv_{\tilde{Y}} = -\frac{1}{\rho}p_{\tilde{Y}} + v\left[v_{\tilde{X}\tilde{X}} + v_{\tilde{Y}\tilde{Y}}\right] + g\beta(T - T_c) - \frac{v}{\kappa}v, \tag{3}$$

$$uT_{\tilde{X}} + vT_{\tilde{Y}} = \alpha\left[T_{\tilde{X}\tilde{X}} + T_{\tilde{Y}\tilde{Y}}\right]. \tag{4}$$

Boundary conditions

The associated boundary conditions are as follows:

Velocity boundary constraints on all boundaries of enclosure:

$u\left(\tilde{X}, \tilde{Y}\right) = 0 = v\left(\tilde{X}, \tilde{Y}\right),\ 0 \le \tilde{X} \le L,\ 0 \le \tilde{Y} \le L$

Themal boundary constraints on top an bottom horizontal walls:

$T(X, L) = T_h$ and $T\left(\tilde{X}, 0\right) = T_h$

On the left and right vertical walls $T\left(0, \tilde{Y}\right) = T_c$ and $T\left(L, \tilde{Y}\right) = T_c$

On the remaining portion at top and bottom horizontal wall

$$\frac{\partial T}{\partial y}\left(\tilde{X}, L\right) = 0 \text{ and } \frac{\partial T}{\partial y}\left(\tilde{X}, 0\right) = 0. \tag{5}$$

$$\breve{X} = \frac{\tilde{X}}{L}, \breve{Y} = \frac{\tilde{Y}}{L}, \breve{U} = \frac{uL}{\alpha}, \breve{V} = \frac{vL}{\alpha}, \breve{P} = \frac{pL^2}{\rho\alpha^2}, \breve{\theta} = \frac{T - T_c}{\Delta T}. \tag{6}$$

Using variables defined in Eq. 6, Eqs 2–4 take the following forms:

$$\breve{U}_{\breve{X}} + \breve{V}_{\breve{Y}} = 0, \tag{7}$$

$$\breve{U}\breve{U}_{\breve{X}} + \breve{V}\breve{U}_{\breve{Y}} = -\breve{P}_{\breve{X}} + \mathrm{Pr}\left[\breve{U}_{\breve{X}\breve{X}} + \breve{U}_{\breve{Y}\breve{Y}}\right] - \frac{\mathrm{Pr}}{Da}\breve{U}, \tag{8}$$

$$\breve{U}\breve{V}_{\breve{X}} + \breve{V}\breve{V}_{\breve{Y}} = -\breve{P}_{\breve{Y}} + \mathrm{Pr}\left[\breve{V}_{\breve{X}\breve{X}} + \breve{V}_{\breve{Y}\breve{Y}}\right] + Ra\mathrm{Pr} - \frac{\mathrm{Pr}}{Da}\breve{V}, \tag{9}$$

$$\breve{U}\breve{\theta}_{\breve{X}} + \breve{V}\breve{\theta}_{\breve{Y}} = \breve{\theta}_{\breve{X}\breve{X}} + \breve{\theta}_{\breve{Y}\breve{Y}}. \tag{10}$$

The associated boundary conditions in a dimensionless form are as follows:

On each of the six walls forming the boundaries: $\breve{U}(\breve{X}, \breve{Y}) = 0 = \breve{V}(\breve{X}, \breve{Y}),\ 0 \le \breve{X} \le 1,\ 0 \le \breve{Y} \le 1$

On the rectangular at the top and bottom horizontal walls: $\breve{\theta}(\breve{X}, 1) = 1$ and $\breve{\theta}(\breve{X}, 0) = 1$

On the left and right vertical walls,

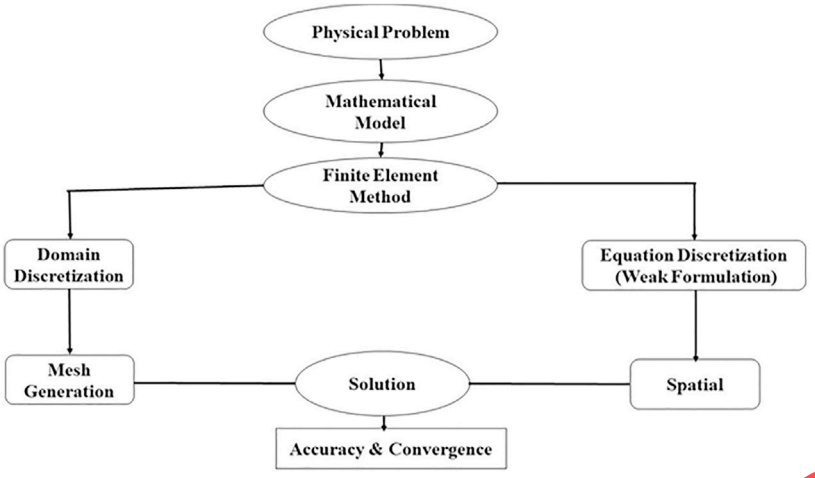

FIGURE 3
Schematic diagram of the finite element method.

TABLE 2 Grid convergence analysis for the mean Nusselt number with the fixed values of $Pr = 0.710, Da = 10^{-3}$, and $Ra = 10^3$.

Refinement level	Nu_{avg}
$R.L_1$	6.5552
$R.L_2$	6.7927
$R.L_3$	6.9533
$R.L_4$	6.9589
$R.L_5$	7.0229
$R.L_6$	7.0661
$R.L_7$	7.2175
$R.L_8$	7.2859
$R.L_9$	7.2859

$$\breve{\theta}(0,\breve{Y}) = 0 \text{ and } \breve{\theta}(1,\breve{Y}) = 0. \tag{11}$$

On the remaining portion at top and bottom horizontal walls $\breve{\theta}\breve{Y}(\breve{X},1) = 0$ and $\breve{\theta}_{\breve{Y}}(\breve{X},0) = 0$.

Based on the aforementioned calculations, the involved physical parameters are the Darcy number $Da = \kappa/L^2$, Prandtl number $\mathrm{Pr} = \upsilon/\alpha$, and Rayleigh number

$$Ra = g\beta\Delta TL^3/\alpha\upsilon, \tag{12}$$

where κ is the permeability of the porous medium, υ is kinematic viscosity, g is gravitational acceleration, α is thermal diffusivity, and β is the thermal expansion coefficient.

The rate of heat transfer computed at the top and bottom horizontal rectangular walls is expressed in terms of the local Nusselt number (Nu_{Local}) as:

$$Nu_{Local} = -\frac{\partial\breve{\theta}}{\partial n}, \tag{13}$$

where n denotes the normal direction on a plane, while the local Nusselt number (Nu_{Local}) is integrated along the bottom horizontal wall and circular cylinder to get the mean Nusselt number (Nu_{Avg}), which is described by:

$$Nu_{Avg} = \frac{1}{s}\int_s Nu_{Local}\, dS, \tag{14}$$

where "s" is the surface of the heated walls. In addition to the aforementioned quantities, it is interesting to compute and examine the global quantity, namely, the total kinetic energy, which is mathematically expressed as follows:

$$K.E = \frac{1}{2}\int_\Omega \|\xi\|^2\, d\Omega, \tag{15}$$

where $\xi = (\widehat{U},\widehat{V})$ represents the vector of velocity.

Solution methodology

The transport mechanism of fluids in simple, confined geometries is easily managed by exact approaches and traditional schemes. However, most of the problems in nature arise due to intricate structural designs, so previously implemented exact schemes are unable to solve them. For this purpose, the analytical approaches are found to be the best for solving these problems. Specifically discussing the irregular shapes, the flow phenomenon is efficiently tackled by a versatile method known as the finite element method. In this procedure, the domain is divided into small portions, and variables of interest are computed at an element level. Depending

10.3389/fphy.2022.1032437

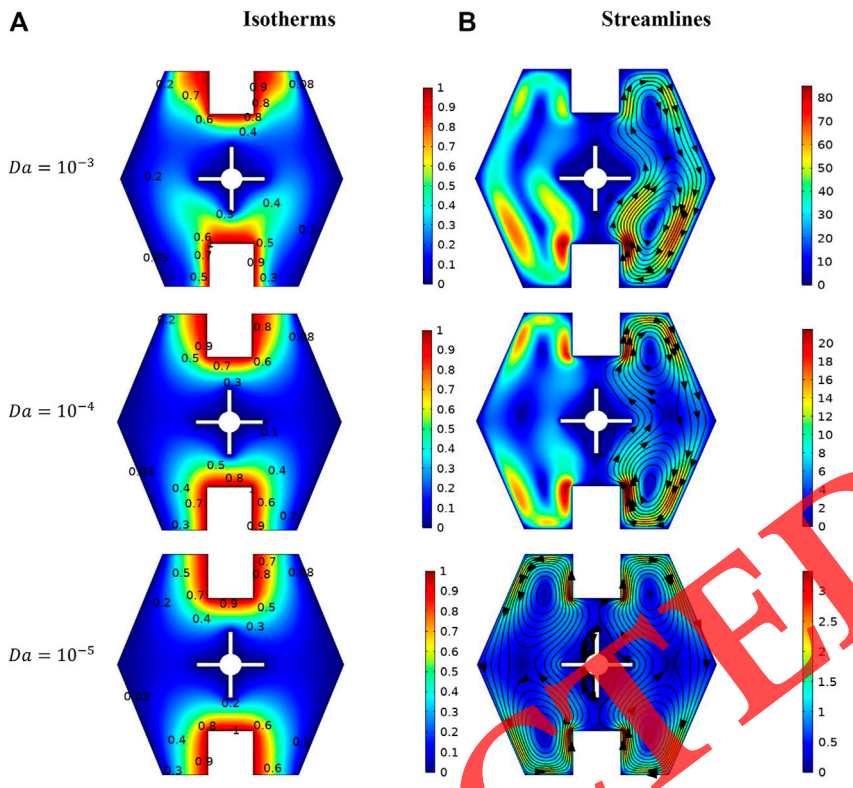

FIGURE 4
(A,B) Isotherms (left) and streamlines (right) under the influence of *Da* at $Ra = 10^3$ and $Pr = 0.710$.

on the field variables, degrees of freedom are computed at different refinement levels as shown in Table 1 and interpolated by utilizing a stable element pair. The governing problem discussed here comprises of pressure which is approximated by linear polynomials, whereas the rest of the distributions are approximated by quadratic polynomials. Discretization of the domain is manifested in Figure 2, which describes hybrid meshing at a coarse level with triangular and rectangular elements. Afterward, a system of non-linearized equations is formed and solved by a direct solver known as PARADISO. The steps involved in the scheme are presented in Figure 3. The convergence criterion adjusted for non-linear iterations is as follows:

$$\left|\frac{\chi^{n+1} - \chi^{n}}{\chi^{n+1}}\right| < 10^{-6},$$

where χ characterizes the general solution component.

Grid convergence

To show the efficiency of the obtained results, the grid convergence test is performed at various grid levels and with the fixed values of $Pr = 0.71, Ra = 10^3$, *and* $Da = 10^{-3}$, as shown in Table 2. For this purpose, the average Nusselt number is computed. It is seen that at levels 8 and 9, the values of the previously mentioned quantities of engineering interest show agreement with each other.

Results and discussion

This section is highlighted to adumbrate the influence of sundry factors on associated distributions and quantities of engineering interest. First, the problem of structuring is manifested in dimensionless PDEs, and then finite element computations are performed to find a solution. Figures 4A, B show the change in momentum and thermal fields in view of streamlines and isotherm patterns. Figure 4A illustrates the change in temperature *via* isotherm contours against *Da*. It is noticed that, at $Da = 10^{-3}$, the magnitude of isotherms increases gradually against (*Da*) because voids in the medium enhance which causes disturbance in the flow and increases the momentum profile. From the prospective that the temperature field is concerned against (Da), it is adhered that two regions are developed around the fin which show intense trajectories against the increasing magnitude of (Da) due to an uplift in kinetic energy and associated heat flux. Variations

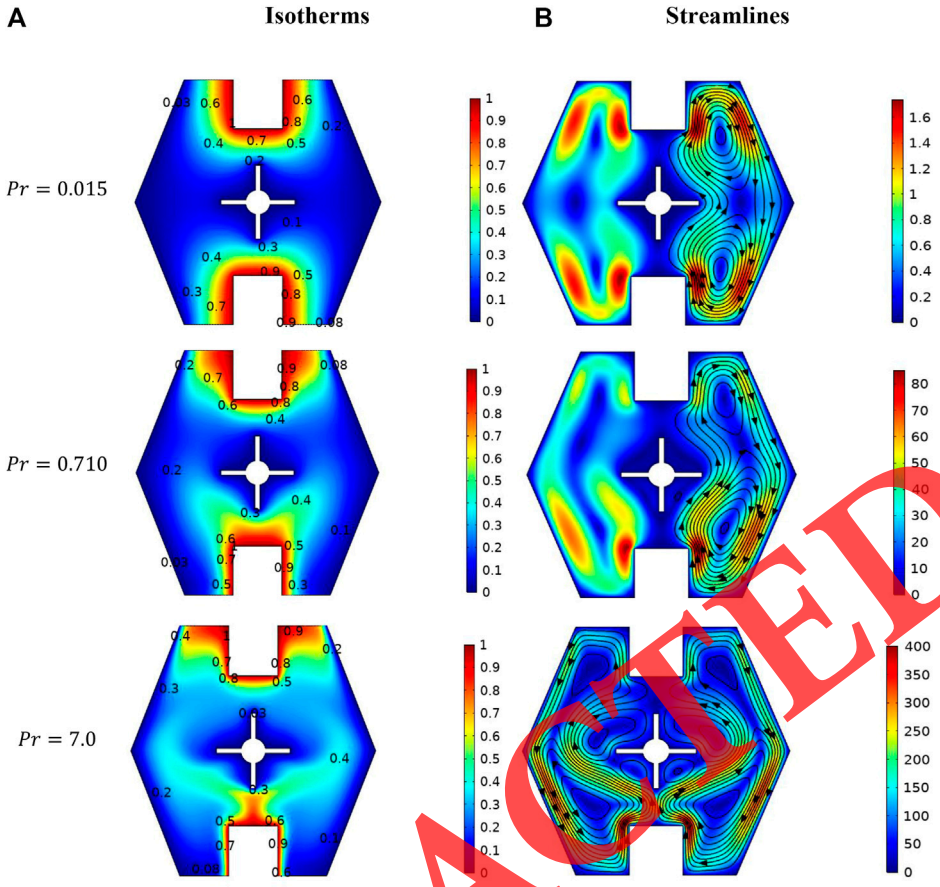

FIGURE 5
(A,B) Isotherms (left) and streamlines (right) for the variation in *Pr* at $Ra = 10^3$ and $Da = 10^{-3}$.

in the temperature profile when $Da = 10^{-3}$–10^{-5} are evaluated *via* streamlines, as shown in Figure 4B. It is divulged that at $Da = 10^{-4}$, streamlines rise from the lower heated rectangle toward the cold fin and form eddies in an elliptical shape. Furthermore, escalation in streamline density is observed at lower values of $Da = 10^{-5}$, and four eddies in the left and right ribs of the enclosure with clockwise and anti-clockwise oval rotations are formed. The impact of the Prandtl number (Pr) on thermal and velocity fields *via* isothermal and streamlines is shown in Figures 5A, B. Since viscous fluid is assumed in the present study, three different magnitudes of (Pr) are taken into account, i.e., $Pr = 0.015$ $(Mercury)$, $Pr = 0.710$ (Air), and $Pr = 7.0$ $(Water)$ while keeping $Ra = 10^3$ and $Da = 10^{-3}$ constant.

In Figure 5A, it is exclusively observed that by upsurging (Pr), the diffusivity of liquid mounts due to which the average kinetic energy elevates, and thus as an outcome, temperature exceeds. It is valuable for indication that at $Pr = 0.015$, the isotherm intensity attaches toward boundaries but contrary aspects are seen at $Pr = 7.00$. Moreover, a variation in the velocity field against the Prandtl number (Pr) *via* streamlines is displayed in Figure 5B. It is noted that in the right-half portion of the enclosure, streamlines move toward the cold fin and form eddies along the cold vertical wall with clockwise rotations. Furthermore, deformation in vortices is observed against the highest magnitude of the Prandtl number $(Pr = 7.0)$.

Figures 6A,B demonstrate variations in the isotherms (left) and streamlines (right) against the Rayleigh number (Ra) ranging from $10^3$to 10^5. The influence of (Ra) on the thermal profile is displayed in Figures 6A, B. It is found that by increasing (Ra), the temperature and momentum of the liquid within the computational domain increase. It is due to this reason that with the increase in (Ra), convective potential rises because (Ra) is directly related to $\Delta \boldsymbol{T}$. Due to this, the motion of particles increases because they start to move with more kinetic energy.

Local heat flux coefficients against (Da) are shown in Figures 7A, B with the fixed values of $Ra = 10^3$ and $Pr = 0.710$. It is measured that the local Nusselt number (Nu_{Loacl}) has been noticeably influenced by (Da) and change in length of the hot wall. In Figure 7A, it is observed that the local Nusselt number (Nu_{Loacl}) generally tends to rise with increasing S values. However, $S < 0.2$ presents the reverse behavior. It is also concluded that the

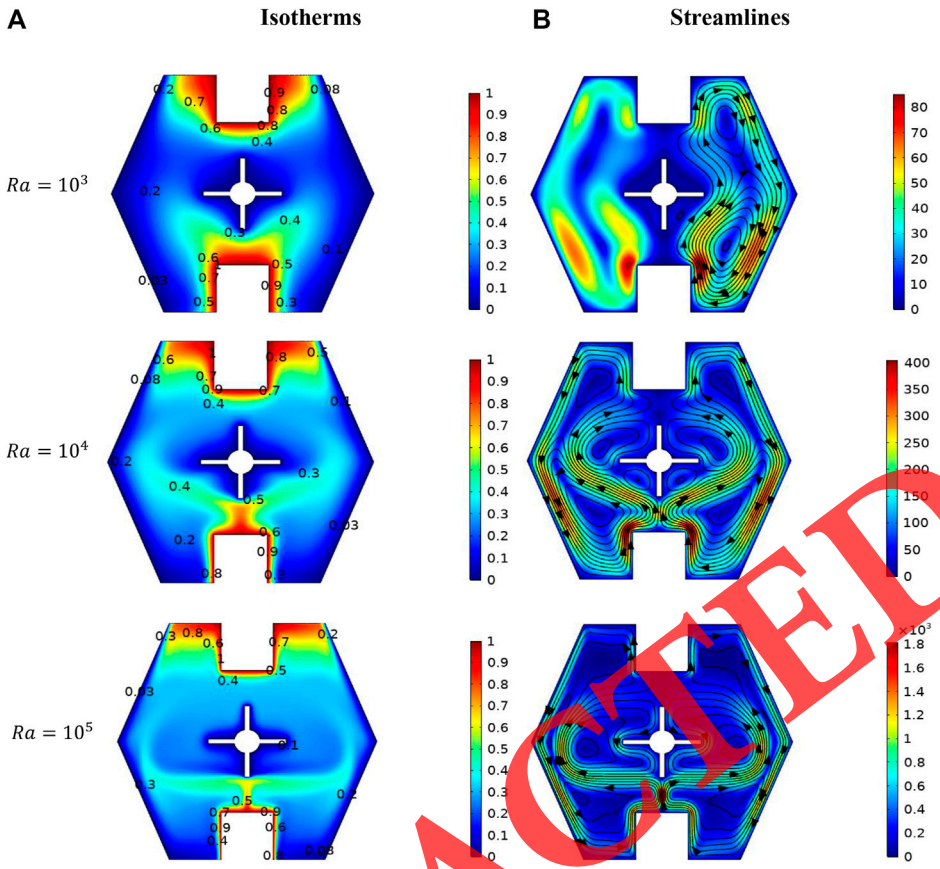

FIGURE 6
(A,B) Isotherms (left) and streamlines (right) for the variation in *Ra* at *Pr* = 0.710 and *Da* = 10^{-3}.

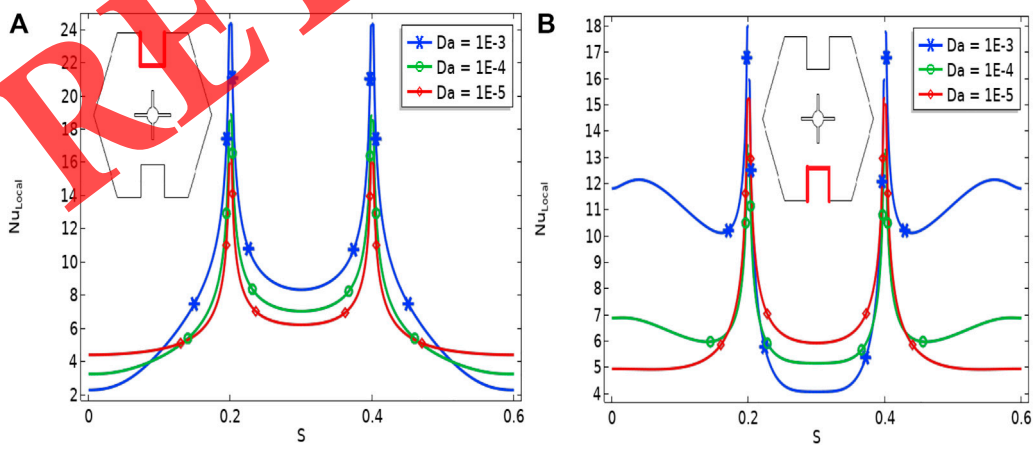

FIGURE 7
(A,B) Local Nusselt number against (Da).

TABLE 3 Variation in the average Nusselt number (Nu_{Avg}) against (Da) and (Ra).

Ra	Da	Nu_{avg}
1E3	1E-3	3.1290
1E4		5.0116
1E5		7.9025
1E3	1E-4	2.8700
1E4		4.3808
1E5		6.1150
1E3	1E-5	2.8568
1E4		2.9060
1E5		5.7240

TABLE 4 Variation in kinetic energy ($K.E$) against the Darcy number (Da).

Da	$K.E_{x=0.1}$	$K.E_{x=0.2}$	$K.E_{x=0.3}$	$K.E_{x=0.4}$	$K.E_{x=0.5}$
1E-3	555.58	1298.0	3443.7	1873.0	22.376
1E-4	4.2842	36.211	83.459	79.799	2.4061
1E-5	0.3200	0.5011	0.8912	1.1976	0.0842

maximum Nusselt number does not change significantly by changing the positions of the hot rectangles. Additionally, it is observed that the Darcy number (Da) has a direct relationship with the local Nusselt number (Nu_{Loacl}), so the highest value of the local Nusselt number (Nu_{Loacl}) is allocated for $Da = 10^{-3}$.

Variation in the average Nusselt number (Nu_{Avg}) against the Rayleigh number (Ra) in the range of ($10^3 \leq Ra \leq 10^5$) is calculated in Table 3. Here, three different values of the Darcy number (Da) have been taken. It is observed from the table that by increasing (Da), Nu_{Avg} also increases, and a similar behavior is depicted against (Ra). The reason behind this fact is that by increasing (Da), the permeability factor enhances due to which kinetic energy increases and heat flux rises.

Demonstration of kinetic energy ($K.E$) against the Darcy number (Da) by drawing cutlines at $0.1 \leq x \leq 0.5$ is shown in Table 4. The result exhibits that (Da) will cause a decrease in the magnitude of kinetic energy ($K.E$). Subsequently, a significant change in kinetic energy is observed at different positions of cutlines, and an increasing behavior toward the center and magnitude of kinetic energy shows a reverse behavior when the fluid interacts with the fin. Additionally, the results show that the kinetic energy at $x = 0.1$ and $Da = 10^{-3}$ was increased 2, 888.12 times more than that at $x = 0.3$.

Table 5 discusses the credibility of present computed findings by measuring the average Nusselt number against the Rayleigh number (Ra) and with fixed values of Pr = 0.7 along with Da = 1. It is observed from the values that the complete match of results is found between published and current works.

Variations in the horizontal component of velocity (u) against decreasing magnitude of the Darcy number (Da) ranging ($10^{-3} \leq Da \leq 10^{-5}$) are illustrated in Figures 8A, B. Here, the cutlines are sketched at $x = 0.2$ (initial of the enclosure) and $x = 0.4$ (near the fin). In Figure 8A, an oscillating aptitude of velocity is attained, and velocity reaches zero at $Y = 0$ and $Y = 1$ due to no-slip velocity at the wall. Additionally, the maximum magnitude in velocity is obtained at $Y = 0.2$, and the minimium value is attained at $Y = 0.9$ (near the upper surface of the enclosure). The Darcy number (Da) evaluates the effectiveness of the inertial forces' increase due to which velocity increases. Also, in Figure 8B, the oscillating behavior of velocity is noted, and velocity reaches zero at $Y = 0$ and $Y = 0.6$ due to the no-slip condition at boundaries. Deviations in the vertical component of velocity (v) against the decreasing magnitude of the Darcy number are illustrated in Figures 8C, D. Here, the cutlines are sketched at $x = 0.3$ and $x = 0.5$. In Figure 8C, an increasing aptitude of velocity is attained, and velocity reaches zero at $Y = 0$ and $Y = 1$ due to no-slip velocity at the wall. Additionally, the maximum magnitude is obtained at $Y = 0.4$, and the minimum value is attained at $Y = 0.01$. It is also noticed that at $Da = 10^{-5}$, no significant change occurs in the vertical velocity component. In Figure 8D, it is found that the maximum temperature is obtained at $Y = 0.25$ and $Da = 10^{-3}$. Since the Darcy number has a direct relationship with temperature, it is also increased by increasing (Da).

Concluding remarks

Natural convective Newtonian fluid flow in a permeable hexagonal enclosure for uniform thermal distributions and by placing a cold fin is analyzed in the current study. The two rectangles at the bottom and top horizontal walls of the cavity are uniformly heated and the adjoining portion is adiabatic, while the inner fin and vertical walls of the cavity are considered the cold domain. The problem is formulated mathematically by capitalizing the governing law, and the solution is implemented as a dimensionless partial differential system. By using the finite element method, computational simulations are carried out. In light of steamlines and isothermal patterns, variations in the associated momentum and temperature are revealed. Quantities of engineering interest like kinetic energy and local and mean heat flux coefficients are measured against dimensionless physical parameters. Some of the main conclusions of the recent research work are as follows:

1) By decreasing the Darcy number (Da), the velocity and temperature distribution reduce which is justified by the streamlines and isotherm patterns.
2) The temperature and velocity distribution are increased when the Rayleigh number (Ra) is increased.
3) By increasing the Prandtl number (Pr), the streamlines and isotherm patterns provide evidence for increased velocity and temperature dispersion.

TABLE 5 Comparison of results with the published literature by measuring the Nusselt number.

Ra	Present result	Shi and Khodadi [44]	Tasnim and Collins [45]	Elatar et al. [46]	Fayz et al. [47]
10^4	2.245	2.247	2.244	2.234	2.245
10^5	4.529	4.532	4.524	4.517	4.522
10^6	8.890	8.893	8.855	8.948	8.835

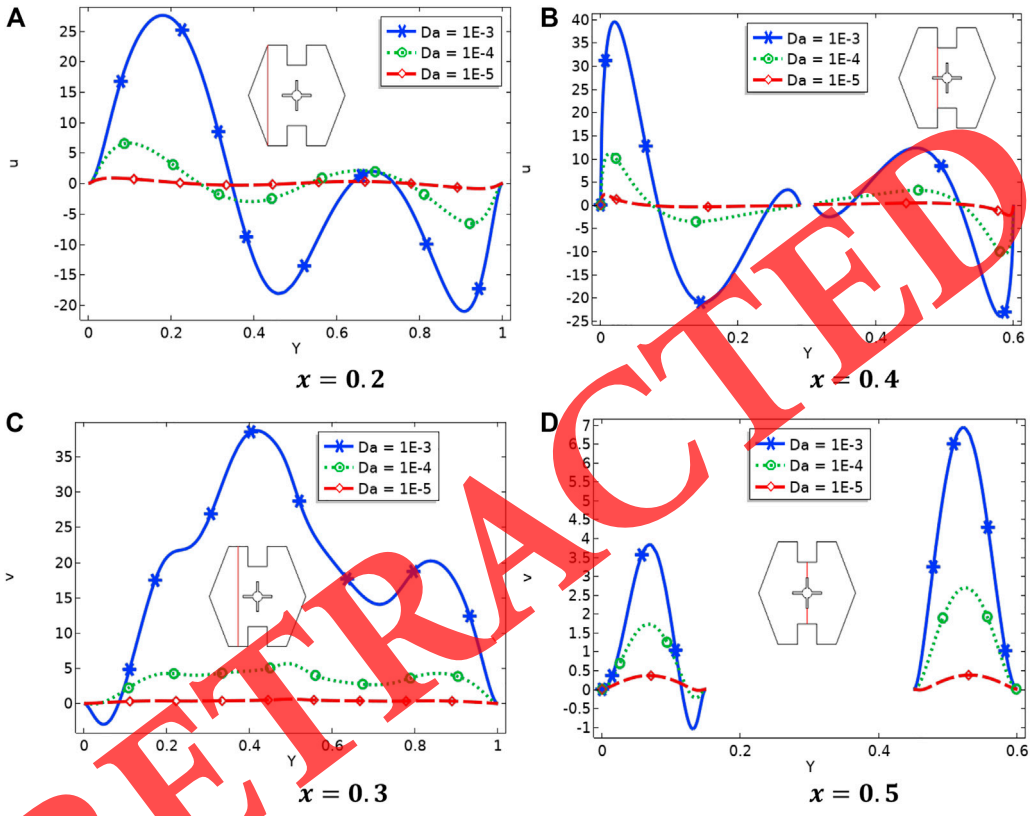

FIGURE 8
(A–F) Variation in velocity and temperature profiles at different positions for various *Da*.

4) The magnitude of kinetic energy shows an increasing behavior against the Darcy number (Da) at different cutlines.
5) The heat flux coefficient shows diminishing aspects against the decrease in the Rayleigh number (Ra).

Data availability statement

The original contributions presented in the study are included in the article/Supplementary Material; further inquiries can be directed to the corresponding author.

Author contributions

All authors listed have made a substantial, direct, and intellectual contribution to the work and approved it for publication.

Conflict of interest

The authors declare that the research was conducted in the absence of any commercial or financial relationships that could be construed as a potential conflict of interest.

Publisher's note

References

1. Brinkman HC. A calculation of the viscous force exerted by a flowing fluid on a dense swarm of particles. *Flow Turbul Combust* (1949) 1(1):27–34. doi:10.1007/bf02120313

2. Beavers GS, Joseph DD. Boundary conditions at a naturally permeable wall. *J Fluid Mech* (1967) 30:197–207. doi:10.1017/s0022112067001375

3. Poulikakos D, Bejan A, Selimos B, Blake K. High Rayleigh number convection in a fluid overlaying a porous bed. *Int J Heat Fluid Flow* (1986) 7:109–16. doi:10.1016/0142-727x(86)90056-1

4. Beckermann C, Ramadhyani S, Viskanta R. Natural convection flow and heat transfer between a fluid layer and a porous layer inside a rectangular enclosure. *J Heat Transfer* (1987) 109:363–70. doi:10.1115/1.3248089

5. Beckermann C, Viskanta R, Ramadhyani S. Natural convection in vertical enclosures containing simultaneously fluid and porous layers. *J Fluid Mech* (1988) 186:257–84. doi:10.1017/s0022112088000138

6. Chen F, Chen C. Experimental investigation of convective stability in a superposed fluid and porous layer when heated from below. *J Fluid Mech* (1989) 207:311–21. doi:10.1017/s0022112089002594

7. Le Breton P, Caltagirone J, Arquis E. Natural convection in a square cavity with thin porous layers on its vertical walls. *J Heat Transfer* (1991) 113:892–8. doi:10.1115/1.2911218

8. Singh A, Thorpe G. Natural convection in a confined fluid overlying a porous layer-a comparison study of different models. *Ind J Pure Appl Maths* (1995) 26:81–95.

9. Webster I, Norquay S, Ross F, Wooding R. Solute exchange by convection within estuarine sediments. *Estuar Coast Shelf Sci* (1996) 42:171–83. doi:10.1006/ecss.1996.0013

10. Goyeau B, Lhuillier D, Gobin D, Velarde M. Momentum transport at a fluid–porous interface. *Int J Heat Mass Transf* (2003) 46:4071–81. doi:10.1016/s0017-9310(03)00241-2

11. Nessrine Z, Ayda B, Hcen D, Sassi BN. Flow and heat transfer during an expansion stroke in a composite fluid/porous system. *J Appl Fluid Mech* (2010) 3:87–95. doi:10.36884/jafm.3.02.11891

12. Kemparaju S, Kumara Swamy HA, Sankar M, Mebarek-Oudina F. Impact of thermal and solute source-sink combination on thermosolutal convection in a partially active porous annulus. *Phys Scr* (2022) 97(5):055206. doi:10.1088/1402-4896/ac6383

13. Reddy NK, Sankar M. Buoyant heat transfer of nanofluids in a vertical porous annulus: A comparative study of different models. *Int J Numer Methods Heat Fluid Flow* (2022). ahead-of-print. doi:10.1108/hff-03-2022-0179

14. Ratouis TMP, Zarrouk SJ. Factors controlling large-scale hydrodynamic convection in the Taupo Volcanic Zone (TVZ), New Zealand. *Geothermics* (2016) 59:236–51. doi:10.1016/j.geothermics.2015.09.003

15. Cheng P. Heat transfer in geothermal systems. *Adv Heat transfer* (1979) 14:1–105. Elsevier. doi:10.1016/s0065-2717(08)70085-6

16. Ingebritsen SE, Sebastian Geiger SH, Driesner. T. Numerical simulation of magmatic hydrothermal systems. *Rev Geophys* (2010) 48:RG1002. doi:10.1029/2009rg000287

17. Molla MM, Saha S, Khan MAI. Natural convection flow in a porous enclosure with localized heating from below. *JP J Heat Mass Transfer* (2012) 6(1):1–16.

18. Alhashash A, Saleh H. Natural convection induced by undulated surfaces in a porous enclosure filled with nanoliquid. *Adv Mech Eng* (2019) 11(9):168781401987528. doi:10.1177/1687814019875284

19. Abedini A, Armaghani T, Chamkha AJ. MHD free convection heat transfer of a water–Fe3O4 nanofluid in a baffled C-shaped enclosure. *J Therm Anal Calorim* (2019) 135(1):685–95. doi:10.1007/s10973-018-7225-8

20. Jetli R, Acharya S, Zimmerman E. Influence of baffle location on natural convection in a partially divided enclosure. *Numer Heat Transfer* (1986) 10(5):521–36. doi:10.1080/10407788608913532

21. Armaghani T, Kasaeipoor A, Izadi M, Pop I. MHD natural convection and entropy analysis of a nanofluid inside T-shaped baffled enclosure. *Int J Numer Methods Heat Fluid Flow* (2018) 28:2916–41. doi:10.1108/hff-02-2018-0041

22. Hussein AK, Ghodbane M, Said Z, Ward RS. The effect of the baffle length on the natural convection in an enclosure filled with different nanofluids. *J Therm Anal Calorim* (2020) 147:791–813. doi:10.1007/s10973-020-10300-1

23. Keramat F, Dehghan P, Mofarahi M, Lee CH. Numerical analysis of natural convection of alumina–water nanofluid in H-shaped enclosure with a V-shaped baffle. *J Taiwan Inst Chem Eng* (2020) 111:63–72. doi:10.1016/j.jtice.2020.04.006

24. Nia SN, Rabiei F, Rashidi MM, Kwang TM. Lattice Boltzmann simulation of natural convection heat transfer of a nanofluid in a L-shape enclosure with a baffle. *Results Phys* (2020) 19:103413. doi:10.1016/j.rinp.2020.103413

25. Ghalambaz M, Mehryan SAM, Alsabery AI, Hajjar A, Izadi M, Chamkha A. Controlling the natural convection flow through a flexible baffle in an L-shaped enclosure. *Meccanica* (2020) 55(8):1561–84. doi:10.1007/s11012-020-01194-2

26. Du R, Gokulavani P, Muthtamilselvan M, Al-Amri F, Abdalla B. Influence of the Lorentz force on the ventilation cavity having a centrally placed heated baffle filled with the Cu– Al2O3– H2O hybrid nanofluid. *Int Commun Heat Mass Transfer* (2020) 116:104676. doi:10.1016/j.icheatmasstransfer.2020.104676

27. Habibzadeh A, Aydin Z, Abbas K. Study of heat transfer in a baffled cavity using nanofluid. *International J Nat Eng Sci* (2013) 7(3):16–20.

28. Hussain A, Afzal A, Mahmood R. Numerical investigation of viscous fluid flow and heat transfer in the closed configuration installed with baffles. *Int J Emerging Multidisciplinaries: Math* (2022) 1(2):49–57. doi:10.54938/ijemdm.2022.01.2.28

29. Benzenine H, Saim R, Abboudi S, Imine O. Numerical simulation of the dynamic turbulent flow field through a channel provided with baffles: Comparative study between two models of baffles: Transverse plane and trapezoidal. *J Renew Energies* (2010) 13(4):639–51.

30. Saravanan S, Vidhya Kumar A. Natural convection in square cavity with heat generating baffles. *Appl Math Comput* (2014) 244:1–9. doi:10.1016/j.amc.2014.06.092

31. Pushpa BV, Sankar M, Makinde OD. Optimization of thermosolutal convection in vertical porous annulus with a circular baffle. *Therm Sci Eng Prog* (2020) 20:100735. doi:10.1016/j.tsep.2020.100735

32. Pushpa BV, Sankar M, Prasanna BMR, Zailan S. Influence of thin baffle and magnetic field on buoyant convection in a vertical annulus. In: *Advances in fluid dynamics*. Singapore: Springer (2021). p. 105–19.

33. Pushpa BV, Sankar M, Mebarek-Oudina F. Buoyant convective flow and heat dissipation of cu–h2o nanoliquids in an annulus through a thin baffle. *J Nanofluids* (2021) 10(2):292–304. doi:10.1166/jon.2021.1782

34. Pushpa BV, Do Y, Sankar M. Control of buoyant flow and heat dissipation in a porous annular chamber using a thin baffle. *Indian J Phys* (2022) 96(6):1767–81. doi:10.1007/s12648-021-02120-2

35. Cuckovic-Dzodzo DM, Dzodzo MB, Pavlovic MD. Laminar natural convection in a fully partitioned enclosure containing fluid with nonlinear thermophysical properties. *Int J Heat Fluid flow* (1999) 20(6):614–23. doi:10.1016/s0142-727x(99)00053-3

36. Beckermann C, Viskanta R, Ramadhyani S. A numerical study of non-Darcian natural convection in a vertical enclosure filled with a porous medium. *Numer Heat transfer* (1986) 10(6):557–70. doi:10.1080/10407788608913535

37. Ali MH, Ahmed AT, Hamada KI. Numerical study of non-darcian natural convection heat transfer in a rectangular enclosure filled with porous medium saturated with viscous fluid. *Tikrit J Eng Sci* (2008) 15(2):90–111. doi:10.25130/tjes.15.2.07

38. Torrance KE, Rockett JA. Numerical study of natural convection in an enclosure with localized heating from below—Creeping flow to the onset of laminar instability. *J Fluid Mech* (1969) 36(1):33–54. doi:10.1017/s0022112069001492

39. Job VM, Gunakala SR, Kumar BR, Sivaraj R. Time-dependent hydromagnetic free convection nanofluid flows within a wavy trapezoidal enclosure. *Appl Therm Eng* (2017) 115:363–77. doi:10.1016/j.applthermaleng.2016.12.084

40. Prasad VR, Rushi Kumar B. Non-similar comutational solutions for double-diffusive MHD transport phenomena for non-newtnian nanofluid from a horizontal circular cylinder. *Nonlinear Eng* (2019) 8:470–85. doi:10.1515/nleng-2018-0035

41. Shah IA, Bilal S, Ali A, Omri M, Bouslimi J, Khan NZ. Significance of cold cylinder in heat control in power law fluid enclosed in isosceles triangular cavity generated by natural convection: A computational approach. *Alexandria Eng J* (2022) 61(9):7277–90. doi:10.1016/j.aej.2021.12.071

42. Bilal S, Zeb Khan N, Ali Shah I, Jan A, Ali A, Bilal Riaz M. Numerical study of natural convection of power law fluid in a square cavity fitted with a

uniformly heated T-fin. *Mathematics* (2022) 10(3):342. doi:10.3390/math10030342

43. Basak T, Roy S, Paul T, Pop I. Natural convection in a square cavity filled with a porous medium: Effects of various thermal boundary conditions. *Int J Heat Mass Transf* (2006) 49:1430–41. doi:10.1016/j.ijheatmasstransfer.2005.09.018

44. Shi X, Khodadadi JM. Laminar natural convection heat transfer in a differentially heated square cavity due to a thin fin on the hot wall. *J Heat Transfer* (2003) 125:624–34. doi:10.1115/1.1571847

45. Tasnim SH, Collins MR. Numerical analysis of heat transfer in a square cavity with a baffle on the hot wall. *Int Commun Heat Mass Transfer* (2004) 31:639–50. doi:10.1016/s0735-1933(04)00051-x

46. Elatar A, Teamah MA, Hassab MA. Numerical study of laminar natural convection inside square enclosure with single horizontal fin. *Int J Therm Sci* (2016) 99:41–51. doi:10.1016/j.ijthermalsci.2015.08.003

47. Fayz-Al-Asad M, Sarker MMA, Munshi MJH. Numerical investigation of natural convection flow in a hexagonal enclosure having vertical fin. *J Sci Res* (2019) 11:173–83. doi:10.3329/jsr.v11i2.38797